# Inhibitory Activity and Structural Characterization of a C-Terminal Peptide Fragment Derived from the Prosegment of the Proprotein Convertase PC7†

Surajit Bhattacharjya,‡ Ping Xu,‡ Mei Zhong,§ Michel Chrétien,||,⊥ Nabil G. Seidah,§ and Feng Ni*,‡

*Biomolecular NMR Laboratory, Biotechnology Research Institute, National Research Council of Canada, 6100 Royalmount Avenue, Montreal, Quebec, Canada H4P 2R2, and Biochemical and Molecular Neuroendocrinology Laboratories, Clinical Research Institute of Montreal, 110 Pine Avenue West, Montreal, Quebec, Canada H2W 1R7*

*Received October 14, 1999; Revised Manuscript Received December 23, 1999*

ABSTRACT: Mammalian proprotein convertases (PCs) belong to the family of recently discovered serine proteases responsible for the processing of a large number of precursor proteins into their active forms. The enzymatic activities of the convertases have been implicated in a variety of disease states, such as cancer and infectious and inflammatory diseases. Like many other proteases, PCs are also synthesized as inactive proenzymes with N-terminal extensions as their prosegments. Here, we present the inhibitory activities of a number of "putative" interfacial peptide fragments derived from the proregion of PC7. We found that a peptide fragment corresponding to the C-terminal region (residues 81p−104p, or C24: $E^1$-A-V-L-A-K-H-E-A-V-R-W-H-S-E-Q-R-L-L-K-R-A-K-$R^{24}$) of the PC7 prosegment displays a strong inhibition ($K_i = 7$ nM) of the PC7 enzyme comparable to that of the full-length (104 residue) prosegment. The same 24 residue peptide shows significantly populated helical conformations in an aqueous solution close to the physiological condition. Structure calculations driven by NOE distance restraints revealed a slightly kinked helical conformation for the entire peptide, characterized by many side-chain/side-chain interactions including those involving charged residues E8-R11-E15 and hydrophobic residues W12 and L19. These results suggest that the C-terminal region of the prosegment of PC7 may play a dominant role in conferring the inhibitory potency to the cognate enzyme and this strong inhibitory activity may be a direct consequence of the folded conformation of the peptide fragment in solution. We surmise that such a structure−function correlation for an inhibitory peptide could lead to the design and discovery of molecules mimicking the specific interactions of the PC prosegments for their cognate proteases.

Most of the proteases from all four major classes (thiol, aspartic, serine, and metallo) are synthesized as inactive precursor molecules with N-terminal extensions as their prosegments *(1)*. These prosegments appear to play critical roles in folding, stability, and regulation of the enzymatic activities of the cognate proteases *(1)*. *In vivo* experiments have shown that coexpression of prosegments (either in *cis* as an adjacent peptide or in *trans* as a separate polypeptide) is necessary for the production of active proteases *(2−4)*. Studies with the α-lytic protease *(4)*, subtilisins *(5, 6)*, carboxypeptidase Y *(7)*, and aqualysin *(8)* have illustrated the ability of the proregions to refold the denatured protease domains as intramolecular chaperones. Our interest in the proregions of these proteases stems from their potent and potentially specific inhibitory activities toward their cognate enzymes. Fox et al. *(9)* demonstrated a strong competitive inhibition ($K_i = 0.4$ nM) of the cysteine protease cathepsin B, but not of papain, by a synthetic peptide representing 56 of the 62 residues of the cathepsin B prosegment. Similar observations have been made for the proregions of other classes of proteases *(7, 10−12)*. These results have stimulated a great deal of interest to identify inhibitory motifs in the prosegments of proteases which may be useful for the design of highly selective inhibitors against the respective proteases *(13−16)*.

Mammalian proprotein convertases (PCs)[1] comprise a family of newly discovered calcium-dependent serine endoproteases which are responsible for the posttranslational processing of a variety of higher molecular weight precursor proteins including hormones, neuropeptides, growth factors, cell surface receptors, adhesion molecules, bacterial toxins, and viral glycoproteins *(17, 18)*. The endoproteolytic activity of the convertases is manifested by the cleavage of protein substrates at paired or multiple basic residues *(18)*. This class of enzymes is homologous to bacterial subtilisins and to the yeast prohormone convertase kexin *(18)*. At present, there are seven distinct convertases (PC1/3, PC2, PC4, PC5/6, LPC/PC7, furin, and PACE4) (*19−22*). Like other proteases,

† This work was supported in part by the Protein Engineering Network Centres of Excellence, sponsored by the Government of Canada, by a Medical Research Council Canada Program Grant (No. PG-11474 to N.G.S. and M.C.), and by the National Research Council of Canada (NRCC Publication No. 42942).

* Corresponding author. Fax: (1)(514)496-5143, E-mail: feng.ni@nrc.ca.

‡ Biomolecular NMR Laboratory, National Research Council of Canada.

§ Biochemical Laboratory, Clinical Research Institute of Montreal.

|| Molecular Neuroendocrinology Laboratory, Clinical Research Institute of Montreal.

⊥ Present address: Loeb Health Research Institute at the Ottawa Hospital, 725 Parkdale Ave., Ottawa, ON K1Y 4K9.

[1] Abbreviations: PCs, proprotein convertases; rPC7, rat PC7; NMR, nuclear magnetic resonance; NOESY, nuclear Overhauser effect spectroscopy; NOE, nuclear Overhauser effect; TOCSY, total correlation spectroscopy; TFE, 2,2,2-trifluoroethanol; DSS, 2,2-dimethyl-2-silapentane-5-sulfonic acid.

10.1021/bi9923961 CCC: $19.00 
Published on Web 02/26/2000

PCs are also synthesized as proenzymes with N-terminal prosegments. The prodomains of PC1/3 *(23)*, PC2 *(24)*, kexin *(25)*, and furin *(26, 27)* have been shown to be involved in autoinhibition, folding, and transport mechanisms of the respective proteases. Recently, PC7 and other convertases have been implicated in diseases such as breast cancer, neurological diseases, hypertension, and neoplasia *(28, 29)*. These observations suggest that specific inhibitors against PC7 and other convertases may have high therapeutic value *(30)*. In this respect, inhibitory synthetic peptides derived from the proregions could serve as effective starting point molecules for the design of low molecular weight compounds as drug leads.

Full-length prosegments, of most of the proteases studied so far, do not have well-folded conformations in isolation, with the sole exception of the large prodomain (166 residues) of the α-lytic protease. However, proregions appear to adopt stably folded structures when bound to their cognate protease domains. X-ray crystal structures of several proenzyme and prosegment/protease complexes have revealed regions of multiple interfacial contacts between the prosegments and protease domains *(1, 31−33)*. These unique interfacial interactions between the protein domains have been identified as the main contributing factors to the binding affinities and specificities of the proregions *(34)*. The extensive interfacial contacts can also be potentially utilized to generate synthetic peptides that may display binding and inhibitory properties of the full-length proregions (*15, 16*). Thus, guided by the three-dimensional structure of the subtilisin proregion/catalytic domain complex, we have selected "putative" interfacial peptide fragments from the proregion of rat PC7 (rPC7). In this paper, we describe the inhibitory activity and solution conformations of a synthetic peptide corresponding to the C-terminal (81p−104p, where p stands for the proregion) region of the rPC7 prosegment. This peptide fragment, which we will refer to as C24, shows significantly populated helical conformation in a buffered aqueous solution containing 300 mM NaCl. A dramatic stabilization of the helical conformations was observed in 50% (v/v) 2,2,2-trifluoroethanol, a helix-stabilizing cosolvent *(35, 36)*.

## MATERIALS AND METHODS

*Peptide Synthesis and Purification.* Peptides were synthesized using standard FMOC chemistry at the Sheldon Biotechnology Centre of McGill University (Montreal, PQ). Partially purified peptides (≥70%) were further purified on an HPLC with a preparatory C18 column using a linear gradient of acetonitrile/water mixture containing 0.1% trifluoroacetic acid. The major peak fraction was collected and lyophilized. The masses of the peptides were verified by electrospray mass spectrometry.

Peptide samples for NMR experiments were prepared in 25 mM sodium phosphate at pH 5.8, in 100 mM sodium phosphate containing 300 mM NaCl at pH 5.8, or in 25 mM sodium phosphate containing 50% (v/v) TFE at pH 5.8. The peptide concentrations were typically 1.5 mM in the aqueous salt solution and 1 mM in 50% (v/v) TFE solution. The temperatures were fixed to 283 and 288 K for NMR experiments in aqueous and TFE solutions, respectively.

*Enzymatic Activity and Inhibition Assays.* Media from BSC40 cells infected with VV:rPC7-BTMD *(22)* were 50-fold concentrated and kept in 40% glycerol at −20 °C. Enzymatic activity was determined by cleavage of a fluorogenic synthetic peptide substrate, pERTKR-MCA (Peptide International). The assay starts with adding 5 μL of the concentrated media to a buffer solution consisting of 100 mM Tris−acetate, pH 7.0, 2 mM $Ca^{2+}$, and variable concentrations of pERTKR-MCA in a final volume of 100 μL. Fluorescence was measured at 0, 30, 60, and 90 min using a Perkin-Elmer spectrofluorometer (model LS 50B) set to an excitation wavelength of 370 nm and an emission wavelength of 460 nM. To determine the inhibition constants ($K_i$'s), 15 min before addition of pERTKT-MCA at either 100 μM, 200 μM, or 300 μM, each synthetic peptide was added to the above fluorogenic assay mixtures at various concentrations.

*NMR Experiments.* All the NMR experiments were performed on a Bruker Avance-500 or a Bruker Avance-800 spectrometer equipped with pulse field gradient units. The water solvent resonance was suppressed by the WATERGATE method *(37)*, or by presaturation using a low-power (∼50 db) pulse in 50% aqueous TFE solution, respectively. A purging field gradient pulse and a water flipback pulse were employed for the acquisition of the two-dimensional NOESY and TOCSY data in aqueous solution *(38)*. The mixing times were 80, 150, and 250 ms at 800 MHz and 250 ms at 500 MHz for NOESY experiments and 68 ms for TOCSY executed with the TOWNY-16 *(39)* mixing sequence. Typically, FIDs were collected with 2K data points with 256−512 $t_1$ increments. The NMR data were processed using the XWINNMR software, using $\pi/2$ or $\pi/4$ cosine window functions along both time dimensions.

*Resonance Assignments and Measurement of $^3J_{HN\alpha}$ Coupling Constants.* Sequence-specific assignments of the proton ($^1$H) resonances were achieved using the standard method *(40)* (Tables S1 and S2 in the Supporting Information) through a combined analysis of TOCSY and NOESY spectra. All spin systems were observed, except that of the N-terminal residue, in the TOCSY spectra connecting the NH all the way to remote $C^\delta H$ resonances. The chemical shifts were referenced to internal DSS. The $^3J_{HN\alpha}$ coupling constants were calculated using the method of Titman and Keeler *(41)* (Table S3 in the Supporting Information) for which the anti-phase COSY patterns were produced by an F1-inphase COSY experiment (Xu and Ni, unpublished results).

*Structure Calculations.* The structures were calculated using the distance geometry method, implemented through a VTF protocol, with fixed bond angles and bond lengths, provided in the ECEPP/3 database *(42−44)*. The calculations were driven solely by use of NOE-derived distance restraints without inclusion of any angular or hydrogen bond constraints. NOE intensities were classified into four distance categories: strong, 1.5−2.5 Å; medium, 1.5−3.5 Å; weak, 1.5−4.0 Å; and very weak, 1.5−5.0 Å. All the dihedral angles were varied during structure optimization except for the ω angles which were fixed at a trans conformation ($\omega = 180°$). Several steps of optimizations were carried out with different contact energies and step ranks. The initial round of calculations generated 100 conformers from random starting conformations. The 30 lowest energy conformers with backbone dihedral angles in the allowed region of the Ramachandran map *(45)* were selected for further refinements. Structures with the lowest distance violations were

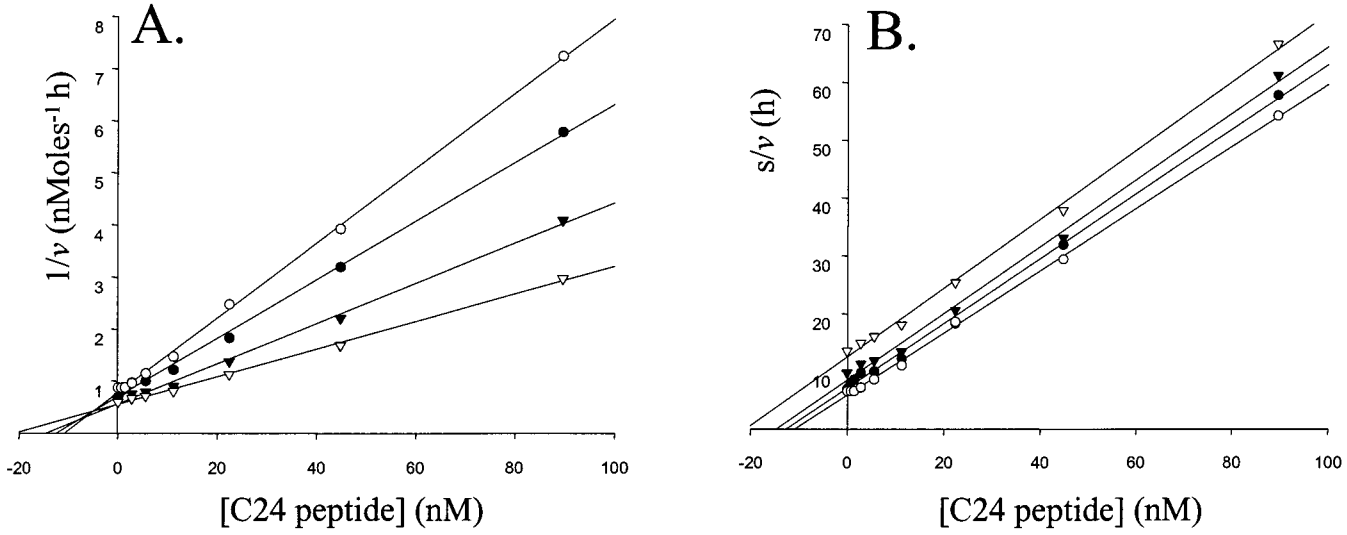


FIGURE 1: Inhibition of rPC7-directed cleavage of pERTKR-MCA by C24. The substrate concentrations used were 75 $\mu$M (○), 100 $\mu$M (●), 150 $\mu$M (▼), and 225 $\mu$M (▽). (A) Dixon plot of 1/velocity ($v$) against C24 concentration at the above stated pERTKR-MCA levels. (B) Cornish−Bowden plot of $s/v$ against C24 concentrations at the various pERTKR-MCA levels.

subjected to independent runs of energy minimization using a distance-restrained Monte Carlo method *(46)*, modified to include the ECEPP/3 force field *(44)*. No electrostatic interactions were taken into consideration during energy minimization. Hydrogen-bonding terms were reduced to 25% of the full strength, thus ensuring that the conformational search was guided primarily by the experimental NOE constraints.

## RESULTS

*Selection of Putative Interfacial Peptides from the Prosegment of PC7.* Identification of the interfacial fragments of the prosegment of PC7 was difficult, since three-dimensional structures are not yet available for proPC7 or any other proprotein convertases. We selected three candidate interfacial peptides from the prosegment of rat PC7 on the basis of the crystal structures of subtilisin/prosegment complexes *(31, 47)*, a bacterial enzyme belonging to the same family of serine proteases *(17)*. These three-dimensional structures revealed three major regions of interfacial contacts between the prosegment and the protease domain of subtilisins. These are made of residues from the N-terminal $\beta$-strand (residues 8p−14p), the C-terminal $\beta$-strand (residues 64p−77p), and a $\beta$-hairpin (residues 36p−51p) of the proregion. Part of the C-terminal $\beta$-strand extends into and occupies the active site cleft of subtilisin, inhibiting the enzymatic activity *(31)*. We assume that similar regions in the prosegment of PC7 may be responsible for binding and inhibition of the enzymatic activity of PC7. Secondary structure predictions of the proregion of PC7 showed that residues 1p−20p and 50p−68p indeed have propensities of $\beta$-strand formation, analogous to the subtilisin prosegment as predicted by the Sompa method *(48)*. However, the C-terminal region of the prosegment of PC7 shows very high propensities for helical conformations. We therefore selected for subsequent studies three peptide fragments corresponding to residues 3p−20p (E-A-G-G-L-D-T-L-G-A-G-G-L-S-W-A-V-H or N20), 50p−68p (G-R-I-G-E-L-Q-G-H-Y-L-F-V-Q-P-A-G-H-G or M18), and 81p−104p (E-A-V-L-A-K-H-E-A-V-R-W-H-S-E-Q-R-L-L-K-R-A-K-R or C24) which may function as the interfacial regions in proPC7.

All three peptide fragments, N20, M18, and C24, were subjected to inhibition studies toward the cognate PC7 enzyme. The N20 and M18 peptides did not yield any measurable inhibitory activities. It was the C24 peptide that turned out to exhibit a very high inhibition of the PC7 enzyme. Kinetic analysis of the inhibition of PC7-directed pERTKR-MCA cleavage by C24 is shown in Figure 1. In Figure 1A, we present the Dixon plots *(49)* of the inverse velocity ($1/v$) as a function of C24 peptide concentrations at various pERTKR-MCA substrate levels. Figure 1B shows the Cornish−Bowden plots *(50)* of the ratio of substrate concentration over velocity ($s/v$) as a function of C24 concentration at various pERTKR-MCA levels. The combination of intersecting lines in Figure 1A with parallel lines in Figure 1B indicates a pure competitive inhibition mechanism with a $K_i$ of ∼7 nM.

The three peptide fragments were further characterized by use of NMR, to screen for a potential correlation between the conformational behavior of the peptides and their inhibitory properties. Three different solvent conditions, namely, a low-salt phosphate buffer containing 25 mM sodium phosphate, or a high-salt phosphate buffer containing 100 mM sodium phosphate and 300 mM NaCl, or an aqueous solution of 25 mM sodium phosphate containing 50% (v/v) TFE, were used to assess the conformations and conformational transitions of the peptide fragments. For both the N20 and M18 peptides, one-dimensional $^1$H NMR spectra were unchanged either in low-salt or in high-salt buffer solutions, indicating the absence of any salt-dependent conformational transitions. In addition, there were intense sequential $C^{\alpha}H$/NH NOEs throughout the sequences and a lack of any medium- or long-range NOEs, either in 100 mM sodium phosphate containing 300 mM NaCl or in 25 mM sodium phosphate containing 50% (v/v) TFE. The $C^{\alpha}H$ proton chemical shifts did not show significant deviations from random coil values nor typical patterns for regular secondary structures, suggesting a lack of folded conformations for these noninhibitory peptides. On the other hand, conformational behaviors of the inhibitory peptide, C24, were markedly different under similar experimental conditions. One-dimensional $^1$H spectra of C24 were well dispersed either

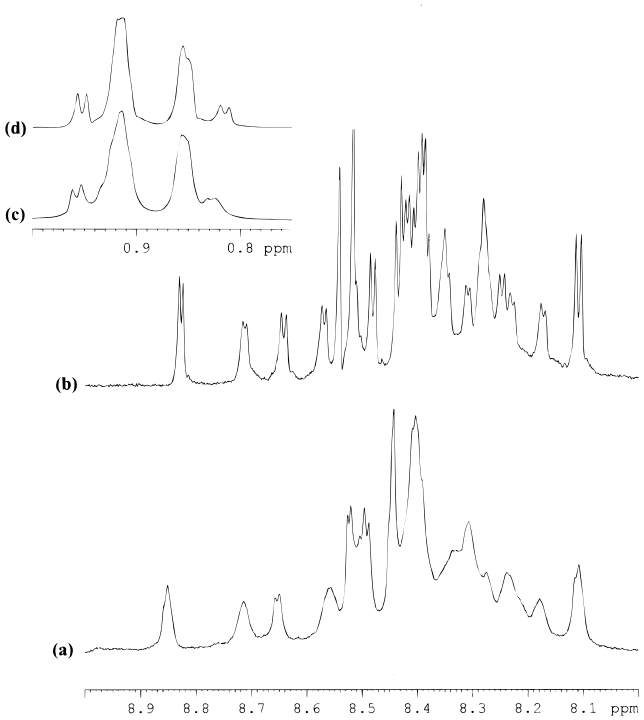


FIGURE 2: One-dimensional $^1$H NMR spectra of the peptide C24 at different salt concentrations. (a and c) Amide and upfield-shifted aliphatic proton resonances in a solution of 25 mM sodium phosphate at pH 5.8, 283 K, respectively. (b and d) Amide and upfield-shifted aliphatic proton resonances in a solution of 100 mM phosphate containing 300 mM NaCl at pH 5.8, 283 K.

in high-salt buffer or in 50% (v/v) TFE solution, in contrast to the two noninhibitory peptides, N20 and M18. In addition, there were a large number of NOE peaks correlating the backbone/backbone, backbone/side-chain, and side-chain/side-chain proton resonances, strongly indicating the presence of folded conformations for peptide C24 in solution.

*Conformation of the Highly Inhibitory C24 Peptide in Aqueous Solution.* The conformation of the C24 peptide was examined in detail in order to gain further insights into the inhibitory activity of this unique region of the PC7 prosegment. Figure 2 shows the amide proton resonances in the one-dimensional proton NMR spectra of the C24 peptide at different salt concentrations. At a low salt concentration, i.e., in a buffer of 25 mM sodium phosphate, at pH 5.8, there is a considerable broadening and poor dispersion of all the amide proton resonances (Figure 2a). Line widths and spectral dispersions were independent of the concentrations of the peptide, precluding the effect of peptide aggregation. The resonance broadening is, therefore, a result of dynamic exchange over different populations of conformations the C24 peptide may assume in solution. An increase in the salt concentration, i.e., in a buffer of 100 mM sodium phosphate and 300 mM NaCl, appears to induce a conformational transition toward a more structured state, which is indicated by a larger resonance dispersion and narrower line widths of the NH resonances (Figure 2b). Enhanced side-chain/side-chain interactions at higher salt concentrations were also indicated by an upfield shift of the aliphatic side-chain resonances (Figure 2c,d). No spectral changes were observed with a further increase of the NaCl concentration up to 600 mM, suggesting the completion of the conformational transition. Therefore, further structural characterization of the C24 peptide in aqueous solution was performed in 100 mM sodium phosphate buffer containing 300 mM NaCl.

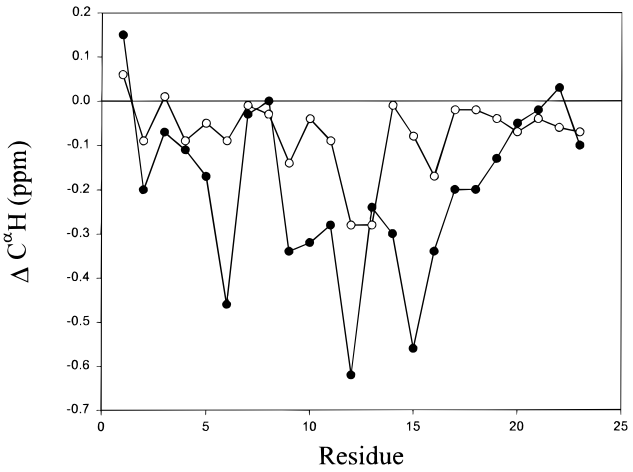


FIGURE 3: Chemical shift deviations of the C$^\alpha$H protons of the C24 peptide in solutions of (○) 100 mM sodium phosphate containing 300 mM NaCl at pH 5.8, 283 K, and (●) 25 mM sodium phosphate containing 50% (v/v) TFE at pH 5.8, 288 K.

Figure 3 shows the deviation of the C$^\alpha$H proton chemical shifts from random coil values *(51)* for each residue in the C24 peptide. The C$^\alpha$H chemical shifts are exquisitely sensitive to the conformational states of the polypeptide *(52)*. An upfield shift or toward lower chemical shift from random coil values is an indicator of helical structure whereas $\beta$-sheet or extended conformations are characterized by downfield or toward higher chemical shifts. Significant upfield shifts for many of the residues of C24 therefore indicate the preference for helical conformations for these residues. However, the extents of the deviations are not as large as observed for peptide helices within proteins *(52)* or helices in aqueous fluoroalcohols *(35)*, suggesting the existence of other conformations in dynamic equilibrium with the helices.

The scalar coupling constant or $^3J_{HN\alpha}$ between the amide and the C$^\alpha$H proton is another parameter sensitive to secondary structures through a direct correlation with the dihedral angle $\phi$ of the peptide backbone. The $^3J_{HN\alpha}$ value expected for an ideal α-helix is on the order of $\leq$3.9 Hz, whereas for $\beta$-strand conformations $^3J_{HN\alpha} \geq 8.0$ Hz. The $^3J_{HN\alpha}$ values for many residues of C24 can be obtained from the well-resolved proton NMR spectra or from an In-phase COSY spectra (see Materials and Methods). Relatively low $^3J_{HN\alpha}$ values (Table S3), within the range of 5.4−6.5 Hz, were obtained for residues H7, E8, V10, E15, R17, L18, and L19, indicating significant population toward helical conformations for these residues *(53)*. In addition, it has recently been shown that conformational fluctuations about the helical region can even increase the measured $^3J_{HN\alpha}$ in isolated protein fragments to between 6 and 7 Hz as the upper boundary *(54)*. Taken together, significant upfield shifts of the C$^\alpha$H resonances and low $^3J_{HN\alpha}$ values for many of the residues suggest that the C24 peptide has an intrinsic conformational preference toward a helical conformation.

The conformation of the C24 peptide was characterized in more detail from an analysis of the nuclear Overhauser effects (NOEs). There were sequential NH/NH NOE connectivities (Figure 4a) for almost all the residues, with 2 (*i*, *i*+2) NH/NH connectivity between the H13/E15 and K20/A22 residues. Several medium-range NOEs between the

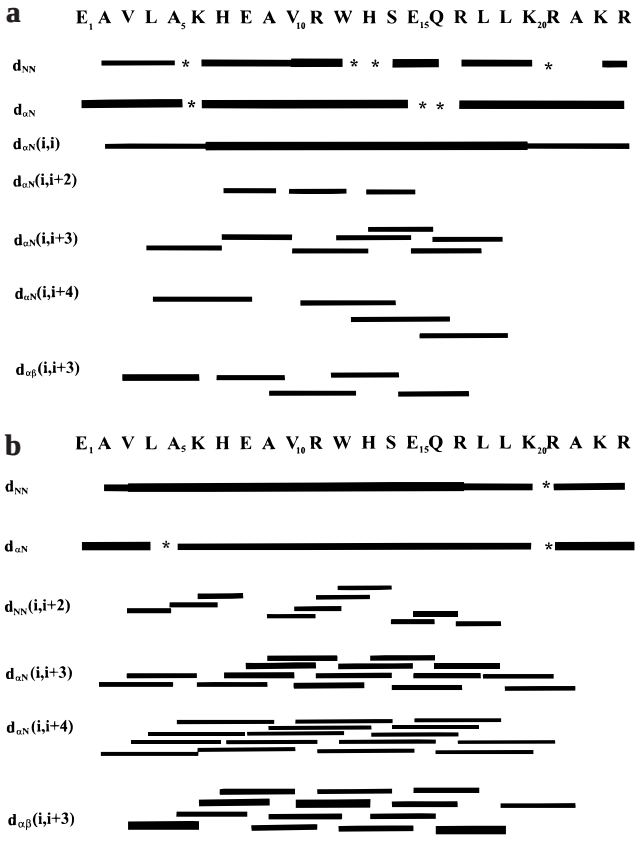


FIGURE 4: Summary of NOEs observed for the C24 peptide in solutions of (a) 100 mM sodium phosphate containing 300 mM NaCl at pH 5.8, 283 K, and (b) 25 mM sodium phosphate containing 50% (v/v) TFE at pH 5.8, 288 K, respectively. The various types of NOEs and their relative intensities are indicated by the thickness of the bar. Asterisks (*) indicate that NOEs could not be assigned unambiguously as a result of spectral overlaps. The amino acid sequence of the peptide is shown at the top.

$C^{\alpha}H$/NH (*i*, to *i*+2, *i*+3, *i*+4) and $C^{\alpha}H/C^{\beta}H$ (*i*, *i*+3) were also observed, which strongly suggests a stable population of α-helical conformations for the C24 peptide. Apart from these backbone NOEs, there were medium-range backbone/side-chain and side-chain/side-chain NOEs involving residues spaced at *i* to *i*+3 or *i*+4, in other words H7 NH/V10 $C^{\delta}H_3$, E8 NH/L4 $C^{\delta}H_3$, E8 NH/A5 $CH_3$, E15 NH/L18 $C^{\delta}H_3$, W12 indole NH protons/E8, A9 side-chain protons (Figure 5), indicating helical conformations along with side-chain packing interactions. The α-helical region of the C24 peptide spans from residues 3 to 20, as defined by a number of medium-range NOEs in that segment (Figure 4a). However, the simultaneous presence of sequential $C^{\alpha}H$/NH NOEs with strong to medium intensities indicates that helical structures must be in exchange with extended conformations, a general feature shared by many potentially folded protein fragments *(53)*.

*Conformations of C24 in 50% TFE.* The helical conformations of C24 observed in the aqueous solution containing salt appear to be dramatically stabilized in a 25 mM sodium phosphate solution containing 50% TFE without NaCl. Larger upfield shifts of the $C^{\alpha}H$ resonances from random coil values were observed, as compared to those of the aqueous solution, indicating a stabilization of the helical conformations in 50% TFE (Figure 3). However, the last four residues (R-A-K-R) at the C-terminus of the peptide and the second residue (A2) at the N-terminus did not show significant chemical shift perturbations, suggesting conformational flexibility for those residues. The $C^{\alpha}H$ protons of residues E8 and A9 also did not exhibit appreciable upfield shifts in the presence of TFE. However, there were many more medium-range NOEs and side-chain NOE interactions for the E8 and A9 residues, indicating helical conformations (*vide infra*).

Some $^3J_{HN\alpha}$ coupling constants could be extracted, i.e., for residues A2, V3, L4, A9, V10, H13, E15, R17, L18, A22, and K23 (Table S3). Unfavorable line widths and spectral overlap preclude the calculation of the $^3J_{HN\alpha}$ values for all the other residues. Residues L4, A9, V10, H13, E15, R17, and L18 show $^3J_{HN\alpha}$ values in the range of 5.0−5.8 Hz, indicating the backbone dihedral angles in the helical region. The end residues A2, A22, and K23 exhibit relatively larger $^3J_{HN\alpha}$ values of 6.17−6.8 Hz, suggesting increased conformational freedom for these residues.

The NOE patterns and intensities observed for C24 in 50% TFE strongly suggest further stabilization of a helical conformation. There is a diminution of the sequential $C^{\alpha}H$/NH NOE intensities with a concomitant increase in sequential NH/NH and intraresidue $C^{\alpha}H$/NH NOE intensities, indicating a significant population of conformations in the helical region of the $\phi$, $\psi$ space *(53)* (Figure 4b). A stable helical conformation is indeed evident by the presence of medium-range $C^{\alpha}H$/NH (*i*, *i*+3 and *i*, *i*+4) NOEs and $C^{\alpha}H/C^{\beta}H$ (*i*, *i*+3) NOEs, encompassing residues V3−K20 (Figure 4b). However, the last four residues (R-A-K-R) and the first two residues may undergo conformational exchange between extended and helical conformations as judged by strong sequential $C^{\alpha}H$/NH and relatively weak NH/NH NOEs.

All the backbone/side-chain and side-chain/side-chain NOEs present in the aqueous solution are preserved in 50% TFE, and along with these, several new NOEs were observed. These new NOEs include those between E8 $C^{\gamma}H$/W12 NH, A9 $CH_3$/W12 NH, V10 $CH_3$/H13 NH, V10 $CH_3$/S14 NH, L18 $CH_3$/E15 NH, L4 $CH_3$/H7 NH, W12 indole NH/L19 $CH_3$, E15 $C^{\gamma}H_2$/L18 $CH_3$, and W12 ring protons/L19 $CH_3$, indicating a stable side-chain/backbone, side-chain/side-chain packing at the middle of the helical structure (Figure 5). The long-range side-chain/side-chain NOEs (*i*, *i*+7) between W12 and L19 could not be assigned unambiguously in the aqueous salt solution as a result of signal overlap. In 50% (v/v) TFE, there were also characteristic side-chain/side-chain NOEs involving R11 $C^{\gamma}H_2$/E15 $C^{\gamma}H_2$, R11 $C^{\gamma}H_2$/E8 $C^{\gamma}H_2$, and E15 $C^{\gamma}H$/R11 $N^{\epsilon}H$ of residues E8, R11, and E15, strongly indicating the formation of salt bridges and hydrogen-bonding interactions in the helical structure. Potential ionic interactions between R11/E15, E8 are also reflected in the chemical shift perturbations of the $C^{\gamma}H$ and $C^{\delta}H$ resonances of E15, E8, and R11, respectively (Table S2). A marked downfield shift was observed for the $C^{\gamma}H_2$ protons of ∼0.2 ppm of E8 and E15 and an upfield shift of ∼0.15 ppm for one of the $C^{\delta}H_2$ proton resonances of R11, characteristic of salt bridge formation in a helical peptide *(55)*. A dramatic downfield shift to 7.82 ppm of the R11 side-chain $N^{\epsilon}H$ resonance and an NOE involving E15 $C^{\gamma}Hs$/R11 $N^{\epsilon}H$ suggest the formation of a hydrogen bond between the R11 $N^{\epsilon}H$ proton and the side-chain C═O group of E15. Observation of the NOEs between E1 $C^{\gamma}H_2$/V3 NH, L4 NH is reminiscent of an N-terminal helix "capping" motif involving residues E1, A2, V3, and L4 *(56)*.

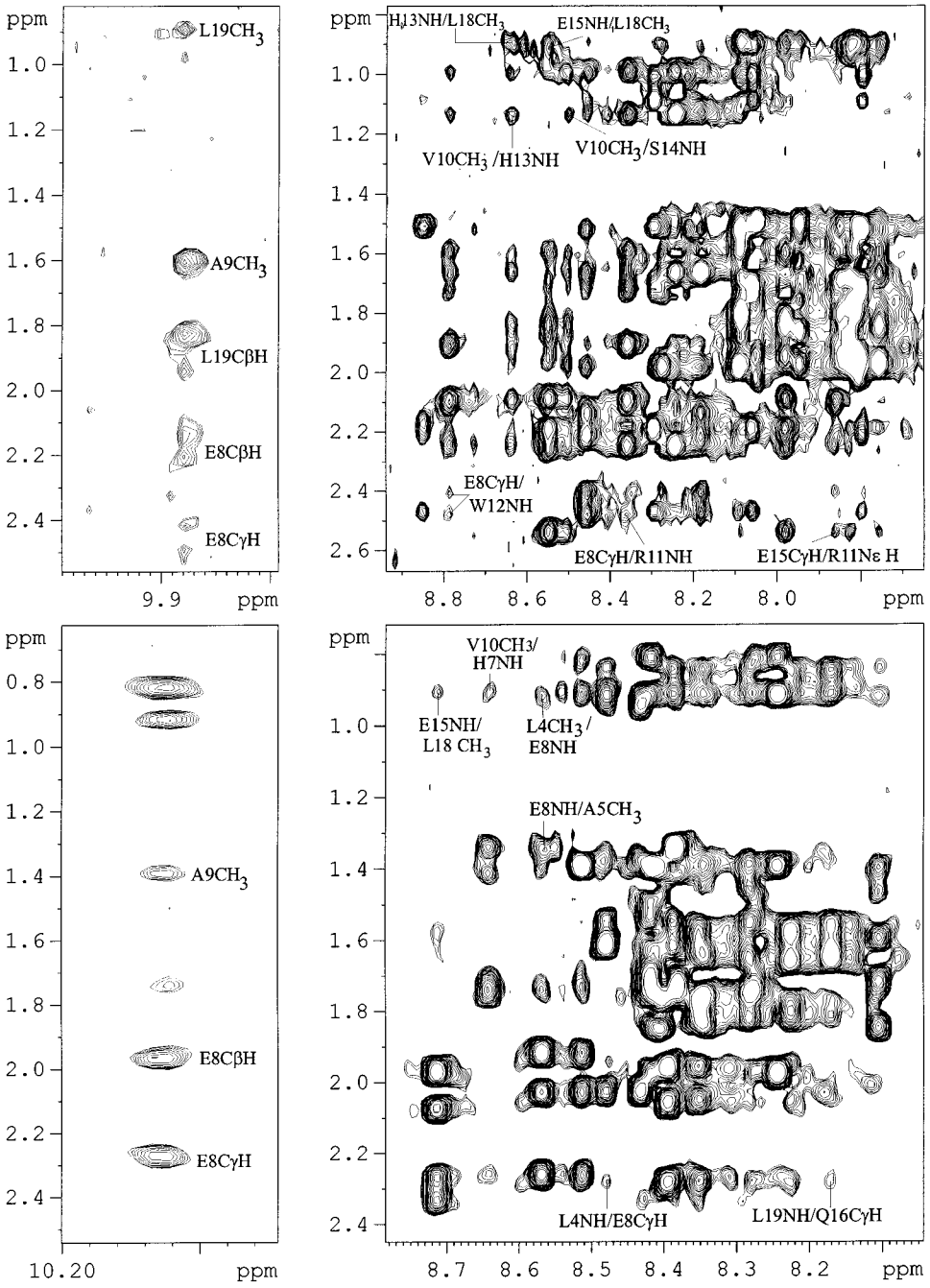


FIGURE 5: Regions of the NOESY spectra of the C24 peptide in solutions of (bottom) 100 mM sodium phosphate containing 300 mM NaCl at pH 5.8, 283 K, and (top) 25 mM sodium phosphate containing 50% (v/v) TFE, at pH 5.8, 288 K, respectively. Spectra show medium- and long-range NOE connectivities between the amide protons and the side-chain proton resonances (right panel); and the W12 indole proton with the side-chain proton resonances of E8, A9, and L19 (left panel).

*Three-Dimensional Structure of the C24 Peptide.* The collection of NMR parameters for the C24 peptide in aqueous buffer and in 50% aqueous TFE solution suggests that the peptide adopts helical conformations under both conditions along with the preservation of some critical backbone/side-chain and side-chain/side-chain interactions. However, there is a marked stabilization of the helical conformation in 50% TFE, which is known to be an agent promoting helix formation in peptide sequences with such intrinsic propensities *(35, 36)*. The presence of a large number of NOEs and side-chain interactions in 50% TFE solution permits us to calculate a high-resolution structure of the peptide on the basis of NOE-derived distance constraints (see Materials and Methods). Table 1 represents a summary of NOE constraints used for structure calculations and structural statistics. Figure 6 shows a superposition of the 20 lowest-energy structures generated through distance geometry and 5 refined structures after Monte Carlo energy minimization. All the ($\phi$, $\psi$) angles are well inside the allowed regions of the Ramachandran map (Table 2). There is a slight kink at the middle of the helix, where W12 possesses a nonhelical dihedral angle ($\phi = -100°$, $\psi = +18°$). This may be effected by the long-range ($i$, $i+7$) aliphatic/aromatic interactions between the W12 ring and the L19 side chain (Figures 5 and 7). Apart from this, there are side-chain interactions in the form of salt bridges and hydrogen bonding involving the ionic groups of residues E8, R11, and E15. The $N^{\epsilon}H$ proton of R11 is

Table 1: Summary of Structural Constraints and Calculation Statistics of the C24 Peptide in 50% (v/v) TFE, pH 5.8 and 288 K

| | |
|---|---|
| distance restraints | |
| unambiguous | 154 |
| intraresidue | 0 |
| sequential | 62 |
| nonsequential [$(i-j) \geq 2$ and $(i-j) \leq 4$] | 87 |
| nonsequential [$(i-j) \geq 5$] | 5 |
| distance restraint violations | |
| number of violations | 12 |
| average violation | ≤0.15 Å |
| maximum violation | ≤0.4 Å |
| deviation from average structure | |
| backbone ($C^{\alpha}$, C′, and N) RMSD in VTF structures | 1.12 Å |
| all atoms RMSD in VTF structures | 2.4 Å |
| backbone ($C^{\alpha}$, C′, and N) RMSD after Monte Carlo minimiation | 0.42 Å |
| all atoms RMSD after Monte Carlo minimization | 1.55 Å |

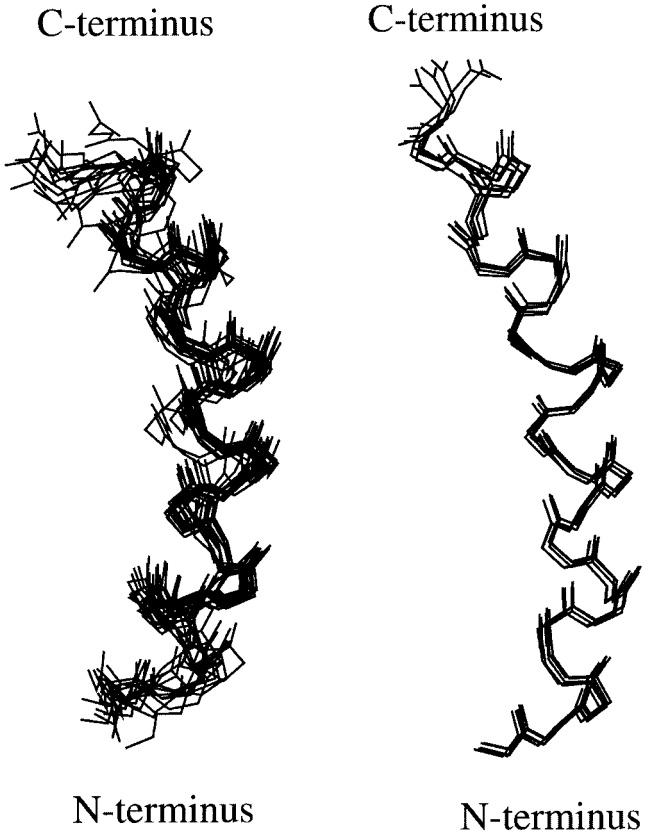


FIGURE 6: Superposition of the backbone atoms ($C^{\alpha}$, C′, and N) of (left) the 20 lowest-energy structures of peptide C24, generated using a distance geometry protocol, and (right) 5 structures generated after further refinement through Monte Carlo minimization.

engaged in hydrogen bonding with the $C^{\gamma}$═O of E15. Analyses of the hydrogen bonding patterns from the Monte Carlo minimized structures reveal that most of the backbone NHs are hydrogen bonded with C═O at $i-4$ positions, leaving two NHs of the N-terminus free, indicating mostly α-helical conformations. However, the L4 and A5 amide protons form $i$ to $i-3$ type hydrogen bonds with the C═O groups of E1 and A2, respectively, suggesting a $3_{10}$-helical turn at the N-terminus. The central kink region around W12 has perturbed hydrogen bonding of Q16 NH and H13 NH engaged in an $i$ to $i-3$ type hydrogen bonding with the C═O of residue V10.

Table 2: Average ($\phi$, $\psi$) Values for the C24 Peptide before and after Monte Carlo Energy Minimization

| residue | $^{av}\phi_{Dg}$ (deg) | $^{av}\psi_{Dg}$ (deg) | $^{av}\phi_{Mc}$ (deg) | $^{av}\psi_{Mc}$ (deg) |
|---|---|---|---|---|
| Ala 2 | −111 ± 15 | −30 ± 7 | −72 ± 5 | −26 ± 3 |
| Val 3 | −74 ± 12 | −35 ± 6 | −67 ± 5 | −26 ± 3 |
| Leu 4 | −72 ± 7 | −36 ± 6 | −77 ± 4 | −32 ± 3 |
| Ala 5 | −108 ± 6 | −30 ± 5 | −68 ± 3 | −38 ± 2 |
| Lys 6 | −72 ± 5 | −36 ± 4 | −72 ± 3 | −32 ± 2 |
| His 7 | −91 ± 5 | −34 ± 5 | −80 ± 2 | −24 ± 3 |
| Glu 8 | −80 ± 4 | −33 ± 3 | −75 ± 2 | −33 ± 2 |
| Ala 9 | −57 ± 5 | −30 ± 3 | −61 ± 2 | −28 ± 2 |
| Val 10 | −79 ± 4 | −37 ± 5 | −92 ± 3 | −41 ± 2 |
| Arg 11 | −74 ± 5 | −31 ± 3 | −65 ± 2 | −30 ± 3 |
| Trp 12 | −95 ± 6 | +28 ± 5 | −100 ± 3 | +18 ± 2 |
| His 13 | −75 ± 5 | −34 ± 2 | −120 ± 3 | −43 ± 2 |
| Ser 14 | −90 ± 4 | −32 ± 4 | −89 ± 2 | −20 ± 2 |
| Glu 15 | −90 ± 5 | −33 ± 3 | −100 ± 3 | −30 ± 3 |
| Gln 16 | −89 ± 4 | −32 ± 5 | −80 ± 3 | −50 ± 2 |
| Arg 17 | −57 ± 5 | −31 ± 3 | −58 ± 2 | −25 ± 3 |
| Leu 18 | −103 ± 6 | −35 ± 5 | −85 ± 3 | −30 ± 2 |
| Leu 19 | −57 ± 4 | −100 ± 6 | −70 ± 2 | −36 ± 3 |
| Lys 20 | −55 ± 5 | −27 ± 8 | −68 ± 4 | −39 ± 4 |
| Arg 21 | −70 ± 7 | −30 ± 9 | −68 ± 5 | −30 ± 3 |
| Ala 22 | −93 ± 10 | −32 ± 11 | −77 ± 5 | −34 ± 3 |
| Lys 23 | −116 ± 10 | +47 ± 13 | −107 ± 8 | +42 ± 6 |

## DISCUSSION

*Role of Residues 81p−104p or the C24 Peptide Fragment for the Inhibitory Activity of the PC7 Prosegment.* The inhibitory proregions of a large number of proteases do not possess a "protein-like" tertiary fold in isolation, making it difficult to characterize the structural requirements of the prosegments in terms of their biological functions. We envisage that the functional determinants of the prosegments could be manifested by the local conformational preferences or secondary structures. In this paper, we have described the inhibitory properties of three peptide fragments and focused on the solution conformation of a highly inhibitory peptide, C24, derived from the C-terminus of the prosegment of rat PC7. Our NMR studies demonstrate that C24 adopts a high population of helical conformations in a salt-containing aqueous buffer solution. Conformational analysis based on $C^{\alpha}H$ chemical shift deviations, $^{3}J_{NH\alpha}$ values, and NOEs indicates that a helical structure encompasses residues 2−20 in aqueous solution. The helical conformations of C24 can be largely stabilized in the presence of 50% TFE with a short helical extension toward the C-terminus as compared with that in aqueous solution. The helical structure is presumably stabilized by "bi-dented" salt bridge interactions and side-chain hydrogen bonding involving residues E8-R11-E15 (Figure 7). Secondary structure predictions of the full-length prosegment indicate a strong intrinsic preference for the helical conformation by the C24 peptide. Interestingly, in the context of the protease, the C-terminal region of the prodomains of subtilisin *(31)* and the α-lytic protease *(33)* forms an extended $\beta$-strand, whereas in carboxypeptidases A and B, helical conformations have been observed *(32)*. The overall similarity in the structural topology of the three prodomains has been hypothesized to have an evolutionary relationship *(57)*. Therefore, the proregions of the proprotein convertases may resemble those of the carboxypeptidases in terms of the conformation of the C-terminal region.

Our results demonstrate that a peptide fragment from the C-terminus of the proregion of rPC7 is sufficient to confer high inhibition toward its cognate protease. Functionally

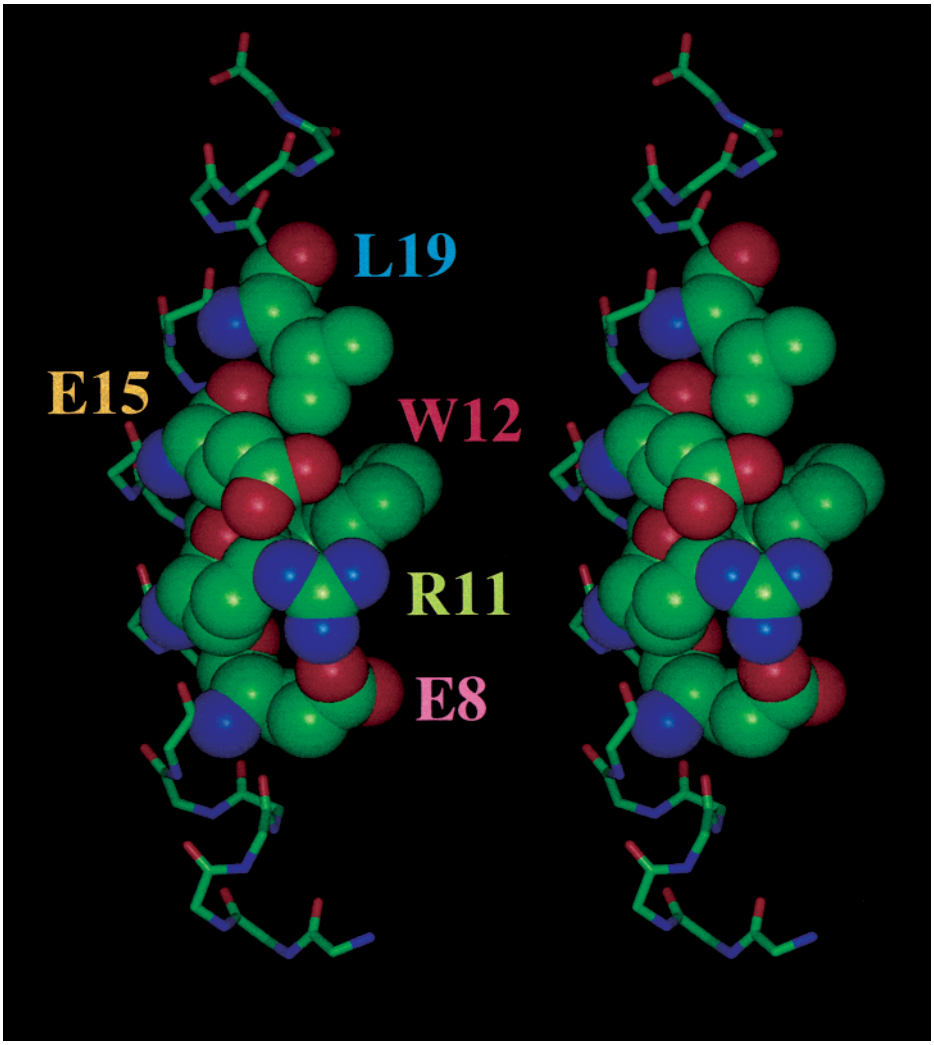


FIGURE 7: Space-filling (in stereo) representation of the side-chain/side-chain contacts in the C24 helical structure. Indicated are ionic interactions involving residues E8, R11, and E15 and long-range hydrophobic packing between the side chains of W12 and L19.

important regions and residues of the cathepsin B prosegment have been identified *(13−16)*, and a highly potent and selective inhibitor has been obtained *(16)*. Attempts have been made to design inhibitors of convertases primarily for PC1 and furin, based on substrate analogues *(58)*. However, these inhibitors have high $K_i$'s and broad binding specificities. On the other hand, the C24 peptide fragment of rPC7 retains a remarkably high inhibitory activity (a low $K_i$). This observation implies that the C-terminal region could be the dominant contributor to the inhibitory affinity of the full-length prosegment of PC7. Studies with the related proregion of mPC1/3 indicated that loss of the C-terminal residues causes a dramatic decrease in the binding ability of the prosegment with the mPC1/3 protease *(23)*. Site-directed mutagenesis experiments with the full-length proregion of the α-lytic protease *(4)* and subtilisin *(2)* have shown the importance of the C-terminal region in inhibition and chaperonin activities. Replacement of the six C-terminal residues of yeast proteinase inhibitor B (YIB2) with those of the proregion of subtilisin BPN′ by site-directed mutagenesis yielded a strong protease-resistant inhibitor of BPN′ *(59)*. Taken together, all these studies suggest a critical role of the C-terminal region of the prosegment for their inhibition activities toward the respective proteases.

*Implications of the Helical Structure for the Inhibitory Activity of the C24 Peptide*. It is intriguing that the C24 peptide has a high inhibitory potency ($K_i$ = 7 nM) comparable to a much longer full-length proregion which has a $K_i$ of ∼1 nM (unpublished results). Such inhibitory functions could be directly related to the observed folded conformations of the peptide in the free state. Although full-length proregions including that of PC7 are devoid of persistent tertiary structure, conformational analysis of the inhibitory peptide fragment C24 indicates the presence of defined secondary structure elements. On the other hand, the noninhibitory peptide fragments N20 and M18 do not show evidence for folded conformations. Recent experiments indicated that functional proteins involved in protein/protein interactions may not need to have classical three-dimensional structures in order to express their biological activities *(60, 61)*. NMR studies performed on such proteins have revealed the presence of transient secondary structures or side-chain/side-chain interactions in the binding regions *(61)*. These results imply that the conformations of the apparently unfolded but bioactive proteins or protein fragments cannot be random, but rather may be closely distributed around the conformation recognized by the target proteins. This kind of conformational order could play a decisive role in determining the strength

of interactions by reducing the loss of conformational entropy upon complexation. Folded conformations have also been observed in the binding interface regions of the peptide fragments derived from cathepsin B *(15)*. Interestingly, histidine-rich human salivary antimicrobial peptides, histatin-3 and histatin-5, are found to be the inhibitors of rPC7 and human furin *(62)*. Both peptides adopt helical conformations in a variety of solvent conditions *(63)*. Taken together, the presence of folded helical conformations and the high binding affinity of the C24 peptide indicate that the free-state conformations may have a dominant role in specifying protein-bound conformations of the active C24 peptide.

## ACKNOWLEDGMENT

We thank Betty Zhu for help in structure calculations and J. Song for a critical reading of the manuscript.

## SUPPORTING INFORMATION AVAILABLE

Two tables showing proton chemical shifts for the C24 peptide in different solutions and one table showing $^3J_{NH\alpha}$ values obtained for the C24 peptide (3 pages). This material is available free of charge via the Internet at http://pubs.acs.org.

## REFERENCES

1. Khan, A. R., and James, M. N. (1998) *Protein Sci. 7*, 815−836.
2. Li, Y., Hu, Z., Jordan, F., and Inouye, M. (1995) *J. Biol. Chem. 270*, 25127−25132.
3. Marie-Claire, C., Ruffet, E., Beaumont, A., and Roques, B. P. (1999) *J. Mol. Biol. 285*, 1911−1915.
4. Sohl, J. L., Shiau, A. K., Rader, S. D., Wilk, B., and Agard, D. A. (1997) *Biochemistry 36*, 3894−3902.
5. Shinde, U., and Inouye, M. (1993) *Trends Biochem. Sci. 18*, 442−446.
6. Wang, L., Ruvino, S., Strausberg, S., Gallagher, T. D., Gilliland, G., and Bryan, P. (1995) *Biochemistry 34*, 15415−15420.
7. Winther, J. R., and Sorensen, P. (1991) *Proc. Natl. Acad. Sci. U.S.A. 88*, 9330−9334.
8. Terada, I., Know, S.-T., and Miyata, Y. (1990) *J. Biol. Chem. 265*, 6576−6581.
9. Fox, T., de Miguel, E., Mort, J. S., and Storer, A. C. (1992) *Biochemistry 31*, 12571−12576.
10. Baker, D., Silen, J. L., and Agard, D. A. (1992) *Proteins: Struct., Funct., Genet. 12*, 339−344.
11. Kojima, S., Minagawa, T., and Miura, K. (1998) *J. Mol. Biol. 277*, 1007−1013.
12. Maubach, G., Schilling, K., Rommerskirch, W., Wenz, I., Schultz, J. E., Weber, E., and Wiederanderanders, B. (1997) *Eur. J. Biochem. 250*, 745−750.
13. Chen, Y., Celine, P., Menard, R., and Storer, A. C., (1996) *FEBS Lett. 393*, 24−26.
14. Chagas, J. R., Martino, F.-D. M., Gauthier, F., and Lalmanach, G. (1996) *FEBS Lett. 392*, 233−236.
15. Yu, Y., Vranken, W., Goudreau, N., de Miguel, E., Magny, M. C., Mort, J. S., Dupras, R., Storer, A. C., and Ni, F. (1998)- *FEBS Lett. 429*, 9−16.
16. Schaschke, N., Assfalg-Machleidt, I., Machleidt, W., and Moroder, L. (1998) *FEBS Lett. 421*, 80−82.
17. Seidah, N. G., and Chrétien, M. (1997) *Curr. Opin. Biotechnol. 8*, 602−607.
18. Nakayama, K. (1997) *Biochem. J. 327*, 625−635.
19. Fuller, R. S., Sterne, R. E., and Thorner, J. (1988) *Science 246*, 482−486.
20. Roebroek, A. J. M., Schalken, J. A., Leunissen, J. A. M., Onnekink, C., Debruyne, F. M. J., Bloemers, H. P. J., and Van de Ven, W. J. M. (1986) *EMBO J. 5*, 2197−2202.
21. Seidah, N. G., Hamelin, J., Mamarbachi, M., Dong, W., Tadros, H., Mbikay, M., Chrétien, M., and Day, R. (1996) *Proc. Natl. Acad. Sci. U.S.A. 93*, 3388−3393.
22. Munzer, J. S., Basak, A., Zhong, M., Mamarbachi, A., Hamelin, J., Savaria, D., Lazure, C., Benjannet, S., Chrétien, M., and Seidah, N. G. (1997) *J. Biol. Chem. 272*, 19672−19681.
23. Boudreault, A., Gautheir, D., and Lazure, C. (1998) *J. Biol. Chem. 273*, 31574−31580.
24. Zhou, A., Paquet, L., and Mains, R. E. (1995) *J. Biol. Chem. 270*, 21509−21516.
25. Powner, D., and Davey, J. (1998) *Mol. Cell. Biol. 18*, 400−408.
26. Anderson, E. D., Van Slyke, J. K., Thulin, C. D., Jean, F., and Thomas, G. (1997) *EMBO J. 16*, 1508−1518.
27. Creemers, J. W. M., Vey, M., Schafer, W., Ayoubi, T. A. Y., Roebroke, A. J. M., Klenk, H.-D., Garten, W., and Van de Ven, W. J. M. (1995) *J. Biol. Chem. 270*, 2695−2702.
28. Seidah, N. G., Mbikay, M., Marcinkiewicz, M., and Chrétien, M. (1997) in *Proteolytic and Cellular Mechanisms in Prohormone and Neuropeptide Precursor Processing* (Hook, Y. H., Ed.) Lands Bioscience Publishers, Springer-Verlag, Heidelberg.
29. Jakson, R. S., Creemers, J. W. M., Ohagi, S., Raffin-Sanson, M. L., Sanders, L., Montague, C. T., Hutton, J. C., and O'Rahilly, S. (1997) *Nat. Genet. 16*, 303−306.
30. Chrétien, M., Cromlish, J. A., and Seidah, N. G. (1997) *Bull. Can. Soc. Biochem. Cell Biol*. 86−96.
31. Gallagher, T., Gilliland, G., Wang, L., and Bryan, P. (1995) *Structure 3*, 907−914.
32. Guasch, A., Coll, M., Aviles, F. X., and Huber, R. (1992) *J. Mol. Biol. 224*, 141−157.
33. Sauter, N. K., Mau, T., Rader, S. D., and Agard, D. A. (1998) *Nat. Struct. Biol. 5*, 945−950.
34. Groves M. R., Coulombe, R., Jenkins, J., and Cygler, M. (1998) *Proteins: Struct., Funct., Genet. 32*, 504−514.
35. Sonnichsen, F. D., Van Eyk, J. E., Hodges, R. S., and Sykes, B. D. (1992) *Biochemistry 31*, 8790−8798.
36. Rajan, R., and Balaram, P. (1996) *Int. J. Pept. Protein Res. 48*, 328−336.
37. Piotto, M., Saudek, V., and Sklenar, V. (1992) *J. Biomol. NMR 2*, 661−665.
38. Fulton, D. B., and Ni, F. (1997) *J. Magn. Reson. 129*, 93−97.
39. Kadkhodaei, M., Hwang, T. L., Tang, J., and Shaka, A. J. J. (1993) *J. Magn. Reson. A105*, 104−107.
40. Wuthrich, K. (1986) *NMR of Proteins and Nucleic Acids*, John Wiley, New York.
41. Titman, J. J., and Keeler, J. J. (1990) *J. Magn. Reson. 89*, 640−646.
42. Ni, F., Meinwald, Y. C., Vasquez, M., and Scheraga, H. A. (1989) *Biochemistry 28*, 3094−3105.
43. Vasquez, M., and Scheraga, H. A. (1988) *J. Biomol. Struct. Dyn. 5*, 705−755.
44. Ni, F., Zhu, Y., and Scheraga, H. A. (1995) *J. Mol. Biol. 252*, 656−671.
45. Ramachandran, G. N., Ramakrishan, C. R., and Sasisekharan, V. (1963) *J. Mol. Biol. 7*, 95−99.
46. Ripoll, D., and Ni, F. (1992) *Biopolymers 32*, 359−365.
47. Jain, S. C., Shinde, U., Li, Y., Inouye, M., and Berman, H. M. (1998) *J. Mol. Biol. 284*, 137−144.
48. Geourjon, C., and Deleage, G. (1995) *Comput. Appl. Biosci. 11*, 681−684.
49. Dixon, M. (1953) *Biochem. J. 55*, 70−72.
50. Cornish-Bowden, A. (1974) *Biochem. J. 1*, 143−144.
51. Merutka, G., Dyson, H. J., and Wright, P. E. (1995) *J. Biomol. NMR 5*, 14−24.
52. Wishart, D. S., Sykes, B. D., and Richards, F. M. (1991) *J. Mol. Biol. 222*, 311−333.
53. Dyson, H. J., and Wright, P. E. (1991) *Annu. Rev. Biophys. Chem. 20*, 519−538.
54. Bolin, K. A., Pitkeathly, M., Miranker, A., Smith, L. J., and Dobson, C. M. (1996) *J. Mol. Biol. 261*, 443−453.
55. Warder, S. E., Zhigang, C., Zhu, Yi., Prorok, M., Castellino, J. F., and Ni, F. (1997) *FEBS Lett. 411*, 19−26.

56. Zhou, H. X., Lyu, P., Wemmer, D. E., and Kallenbach, N. R. (1994) *Proteins: Struct., Funct., Genet. 18*, 1−7.
57. Baker, D. (1998) *Nat. Struct. Biol. 12*, 1021−1024.
58. Jean, F., Basak, A., DiMaio, J., Seidah, N. G., and Lazure, C. (1995) *Biochem. J. 307*, 689−695.
59. Kojima, S., Deguchi, M., and Miura, K. (1999) *J. Mol. Biol. 286*, 775−785.
60. Dyson, H. J., and Wright, P. E. (1998) *Nat. Struct. Biol. 5*, 499−503.
61. Wright, P. E., and Dyson, H. J. (1999) *J. Mol. Biol. 293*, 321−331.
62. Basak, A., Ernst, B., Brewer, D., Seidah, N. G., Munzer, J. S., Lazure, C., and Lajoie, G. A. (1997) *J. Pept. Res. 49*, 596−603.
63. Brewer, D., Hunter, H., and Lajoie, G. (1998) *Biochem. Cell. Biol. 76*, 247−256.

BI9923961